Validation and Comparison of [18F]NaF PET/CT Analysis Methods and Derivation of a Semi-population Input Function for Site Specific Measurements of Bone Formation in a Population with Chronic Kidney Disease Mineral and Bone Disorder

Marie Houmaa Vrist (marvri@rm.dk)
Mayo Clinic Division of Nephrology and Hypertension https://orcid.org/0000-0002-5556-0078
Jesper Nørgaard Bech
University Clinic of Nephrology and Hypertension, Gødstrup Hospital, and Aarhus University
Thomas Guldager Lauridsen
Department of Nephology, Aalborg University Hospital
Claire Anne Fynbo
Department of Nuclear Medicine, Gødstrup Hospital
Jørn Theil
Department of Neclear Medicine, Gødstrup Hospital

Original research

Keywords: NaF, PET/CT, Hawkins, Patlak, semi-population input function, CKD-MBD

Posted Date: September 21st, 2020

DOI: https://doi.org/10.21203/rs.3.rs-72184/v1

Abstract

Background

Methods for assessing bone metabolism which can replace the gold standard bone biopsy are sorely needed in the clinical setting in patients with chronic kidney disease - mineral and bone disorder (CKD-MBD). The aim of the present study was implementation, validation and comparison of non-invasive dynamic and static whole-body (WB) [^{18}F]NaF PET/CT scan methods to replace invasive bone biopsy, used for quantitative analysis of bone clearance in CKD-MBD patients.

Methods

Seventeen patients with CKD-MBD underwent a 60-minute dynamic scan followed by a 30-minute static WB scan. Tracer kinetics in four thoracic vertebrae were analyzed using non-linear regression with the Hawkins model and two different Patlak-analysis methods using image-derived arterial input functions obtained from the left myocardial ventricle and the thoracic aorta. For future use in WB PET/CT scans, we validated the use of a semi-population input function. The resulting kinetic parameters (K_i, K_1, k_2, k_3, k_4, V_0) were compared between the different methods of analysis using the various derived input functions.

Results

Dynamic kinetic results from both standard and single-point Patlak analyses correlate well with non-linear regression analysis, but K_i results using Patlak analysis are generally lower for all tested input functions compared to regression analysis. Single-point Patlak analysis on WB scans correlates well with standard Patlak analysis on dynamic scans but show 13-21% higher K_i-values.

Conclusions

Our results show good correlation between dynamic and static analysis of skeletal plasma clearance but different K_i-values depending on the analysis method and choice of input function used. Thus, WB [^{18}F]NaF PET/CT scans can be applied in future studies, but the results should not be compared uncritically with results obtained using non-linear regression analysis.

Introduction

Fluorine-18 labelled sodium fluoride (^{18}F-NaF) was introduced in the 1960s as a bone-seeking tracer in nuclear medicine[1] and widely used for gamma camera bone scintigraphy, but was later replaced by Technetium-99m labelled diphosphonates in the 1970s. In the past decades, ^{18}F-NaF has been reintroduced in combination with PET/CT.

Chronic kidney disease (CKD) is associated with universal bone abnormalities (renal osteodystrophy) and disturbances in mineral metabolism leading to cardiovascular and extra skeletal calcifications. These processes are caused by common pathophysiological pathways and are defined as a systemic disorder named Chronic Kidney Disease - Mineral and Bone Disorder (CKD-MBD) [2]. Even though bone-related complications have been known in CKD since 1883[3], the key to effective treatment and prevention remains to be found, with this shortcoming possibly attributed to the lack of non-invasive methods available for diagnosing and monitoring CKD-MBD.

Today, bone biopsy is considered the gold standard for analysis [4], but it is invasive, unpleasant and not without risk to the patient. However since the 1990s, non-invasive ^{18}F-NaF PET/CT has shown good potential for monitoring CKD-MBD [5]. Here ^{18}F-NaF, administered as an intravenous bolus injection, diffuses from the plasma into the extra vascular compartment in bones from where it is further incorporated into the bone's hydroxyapatite skeleton as fluoroapatite [6].

The plasma clearance of ^{18}F-NaF to bone [K_i (ml min^{-1} ml^{-1})] reflects changes in either bone blood flow or bone formation rate. Traditionally, non-linear regression analysis with the Hawkins two-tissue, three compartmental, model (Fig. 1) or the Patlak multiple data point graphical method (mp-Patlak), have been used to determine K_i and other kinetic parameters using dynamic data acquisition [7, 8]. K_i-values are shown to correlate well with turnover results obtained by bone biopsies [5]. Both Hawkins and Patlak analysis require dynamic acquisition over a single field-of-view (FOV), typically of 60-minutes duration. Due to restrictions in the axial width of a given scanner (16–25 cm), a single dynamic scan can examine only a selected region of the skeleton, with extended regions of interest requiring multiple scans and tracer injections. This is not only impractical in a clinical setting, but will result in a high radiation dose to the patient. However, modern advances in PET/CT scanner functionality, combining an initial, short duration dynamic acquisition over the heart followed by a series of fast multiple whole-body scans are now available and may soon provide a solution to the problem of extended dynamic scanning. Previously this limitation has been addressed through development of a simplified acquisition and analysis method in which a static, WB ^{18}F-NaF PET scan in combination with a standardized semi-population input function (SPIF), estimates K_i values in multiple bone regions using a single-point graphical analysis (sp-Patlak) [9, 10]. With this method it is possible to perform a 30 minute WB acquisition with site-specific bone analysis using a single tracer injection [9, 11, 12].

The application of a SPIF requires an a priori derived population residual curve. Ideally, a population residual curve should be derived from the relevant population as the curve reflects the tracer distribution in the body and may be subject to vascular changes caused by various diseases. Since the CKD-

MBD population generally has complications with vascular calcifications, it seems possible that a population residual curve for this population may differ from one obtained in an osteoporotic population [13]. To our knowledge, a population residual curve for CKD-MBD patients has not previously been published.

The objectives of this study were threefold: 1) implementation of ^{18}F-NaF PET/CT using the Hawkins method and mp-Patlak analysis for dynamic studies of NaF skeletal plasma clearance, 2) derivation of a CKD-MBD population residual curve for subsequent SPIF construction in combination with venous blood samples to be used as the arterial input function (AIF) for sp-Patlak analysis in WB scans and, 3) comparison and validation of WB scan results with results from dynamic scan analysis.

Materials And Methods

Subjects

Thirty-four chronic dialysis patients (30–80 years) were included, of which 17 participants completed the study (hemodialysis n = 15, peritoneal dialysis n = 2). Exclusion criteria were: pregnancy, participants who suffered from alcohol/drug abuse, were allergic to ^{18}F-NaF or Tetracycline, or in the past three months had had bone fracture, acute myocardial infarction, transitory cerebral ischemia, kidney transplant or parathyroidectomy. Table 1 shows demographics and Fig. 2 shows flowchart for inclusion.

Table 1
Demographics

Demographics (n = 17)	
Age, years	62.5 ± 10.1
Female, % (n)	29.4 (5)
Male, % (n)	70.6 (12)
Body mass index (BMI), kg/m²	24 (23–29)
Dialysis duration, years	2.0 (0.5-3.0)
Cause of kidney failure, % (n)	23.5 (4)
• Hypertension	29.4 (5)
• Diabetic nephropathy	23.5 (4)
• Polycystic kidney disease	5.9 (1)
• Glomerulonephritis	17.6 (3)
• Other/unknown	
Normal distributed data: mean ± SD. Non-normal distributed data: median (25th percentile; 75th percentile)	

During data analysis one patient had to be excluded due to very poor image quality resulting from severe obesity and three patients excluded due to delayed bolus injection and problems with blood sampling.

Image acquisition

PET/CT images were acquired on a Siemens Biograph mCT-4R 64 slice PET/CT scanner with a 22 cm axial FOV. The participants were positioned with the heart and the thoracic vertebrae 7 through 10 (Th7 – Th10) centered in the FOV.

Following an intravenous bolus injection of 150 MBq ^{18}F-NaF flushed with 20 mL isotonic saline, a 60-minute list-mode dynamic scan was acquired followed by a WB scan from the middle of the femur to the vertex of the skull acquired in 6–7 FOVs of 3 minutes per bed position.

Image reconstruction

PET images for dynamic analysis were re-binned into 50-time frames: 20 × 3 s, 12 × 5 s, 4 × 30 s and 14 × 240 s. Reconstruction of PET scans was done using filtered back-projection with a Gaussian filter of 5 mm and matrix size of 256 × 256.

Low-dose CT scans were performed and the images reconstructed in three utilization-dependent series: 1) attenuation correction, 2) localization and identification of thoracic vertebrae in the dynamic scan and 3) localization of the relevant bone regions in the WB scan.

All dynamic images were automatically decay corrected to the study injection time (study reference time). Image data from the WB scan was automatically decay corrected to the start of the WB scan, on average 66 ± 2 minutes post injection, requiring additional decay correction to the study reference time for comparison with dynamic data.

Blood samples

Venous blood samples (5 mL) were collected at -5, 30, 40, 50, 60 and 90 minutes after injection and thereafter centrifuged at 3000 rpm for 10 minutes. The activity concentrations in 1 ml of whole blood and plasma were measured in a well-counter (Perkin Elmer Wizard2® – 2480 Automatic Gamma Counter, USA). The well-counter and PET/CT scanner were cross-calibrated. To convert measured activity from image-derived whole blood to plasma activity curves, plasma to whole blood activity ratios were calculated for each of the samples (Fig. 3).

Image analysis

The PMOD® version 4.003 software (PMOD Technologies LLC, Switzerland) was used for non-linear regression analysis of the dynamic data as well as analysis of the single-point WB data.

The drawing of VOIs, for generation of time activity curves (TACs) from the cardiac left ventricle (LV) or thoracic aorta (AO), was facilitated by summing the relevant time frames with highest activity into one static frame. Contours of the activity within the LV were drawn using the hot contouring tool in PMOD, defined as a percentage of the maximum activity within a box VOI surrounding the LV (typically 45–65%). AO VOIs were drawn using box VOIs (10 × 10 × 30 mm) centered in the aortic lumen (Fig. 4).

For partial volume effect (PVE) and activity spillover correction, VOI contours within the myocardial wall and surrounding the luminal activity in the aorta, were manually drawn using the brush tool on at least 10 axial slices with a voxel-size of 3.2 × 3.2 × 1.4 mm.

Box VOIs were fitted to the trabecular part of the vertebral bodies Th7-Th10, avoiding the endplates and the disk spaces using the CT images as a template. These VOIs were similar for both dynamic and WB studies.

TACs were derived in the PMOD View Module and transferred to the PMOD Kinetic Module for further analysis as described in detail below.

Input functions

Dynamic scan analysis used an image-derived arterial input function (IDAIF) from a VOI placed in the LV and AO as described above.

Errors due to PVE and activity spillover were corrected by calculation of the recovery coefficient β, as described by Cook et al. and Puri et al. [10, 14]

$$R_{LV/AO}(t) = \beta \cdot C_{LV/AO} + (1-\beta) \cdot C_{Bg} \qquad \text{(Eq. 1)}$$

where $R_{LV/AO}$ is activity in the image-derived TAC obtained from the LV or AO, C_{Bg} is the background activity concentration in the surrounding myocardium or aortic wall and $C_{LV/AO}$ is the corrected arterial blood activity concentration in LV or AO. $C_{LV/AO}$ is approximated to activity in venous blood samples 30 minutes after injection [10]. From (Eq. 1), β can be estimated as the mean value of β-coefficients calculated from each of the paired image and blood sample data.

Population residual curves

β-corrected IDAIFs were scaled to a reference dose of 150 MBq and used to generate a residual curve for each participant. The residual curve represents the sum of the early fast exponentials and was derived by subtracting the terminal exponential from the entire image-derived curve. The residual curves were averaged to define the population residual curve in three different ways: 1) Population residual 1 – all residual curves were averaged with *no time adjustment* of the peak (LV: n = 12; AO: n = 11), 2) Population residual 2 – all residual curves were selected but were adjusted so that the times of peak count rate for all curves were coincident with the most frequent unadjusted peak time (LV: 16.5 s; AO: 19.5 s) and, 3) Population residual 3 - only unadjusted residual curves which peaked at the most frequent time frame were selected (n = 6).

For WB analysis we used a SPIF as previously described by Blake et al. [9]. The selected population residual curve was scaled for the patient injected activity and added to the terminal exponential of the plasma TAC to define the 0–60 minute and 0–90 minute SPIF for each subject.

Skeletal plasma clearance analysis

The skeletal plasma clearance [K_i (ml min^{-1} ml^{-1})] was calculated as the mean value of four thoracic vertebrae (Th7-Th10) for the systematic application of three different analytic methods and input functions as described below.

Hawkins model: Non-linear regression analysis

PMOD software was used to perform two-tissue compartmental model dynamic analysis of NaF-turnover as described by Hawkins et al.[7]. The exchange of ^{18}F-NaF between the three compartments (plasma, extravascular and bone) is described by the kinetic parameters (K_i, K_1-k_4, V_0) (Fig. 1), where K_i is defined as:

$$K_i = \frac{K_1 k_3}{k_2 + k_3}. \qquad \text{(Eq. 2)}$$

K_i was calculated for two different predefined values of the percentage of ^{18}F-NaF present in the extravascular compartment V_0: 1) previously published population mean value V_0 = 0.43 [11] and 2) the mean value for this study data V_0 = 0.51, obtained from data analysis performed without a

predefined value.

The fractional blood volume was fixed at 5%.

Patlak: multiple-point graphical analysis

Assuming the efflux rate constant k_4 to be negligibly small ($k_4 \approx 0\ min^{-1}$), mp-Patlak graphical analysis provides a simpler alternative analysis method for measuring K_i as described by Eq. 3 [8, 15].

$$\frac{C_{Bone}(T)}{C_{Plasma}(T)} = K_i \frac{\int_0^T C_{Plasma}(t)\,dt}{C_{Plasma}(T)} + V_0 \qquad \text{(Eq. 3)}$$

This equation approximates a straight-line fit with K_i as the slope. C_{Bone} and C_{Plasma} are the respective concentrations of tracer bound in bone and freely diffusible in plasma. V_0 is the intercept of the ordinate and represents the extra vascular compartment in the bone.

K_i was calculated from the 60-minute dynamic PET/CT scan using a bone TAC and the various image-derived AIFs with and without data from venous blood samples.

Patlak: single-point graphical analysis

For calculation of the straight-line function for analysis, the sp-Patlak model requires a single data point using activity measured in a selected bone region combined with a previously determined value of the intercept (V_0).

The present study compared three different values of V_0 applied in sp-Patlak: a mean value of 0.43, as previously published for mp-Patlak analysis of lumbar vertebrae[11] and two mean values obtained from this study; $V_0 = 0.64$ when data were analyzed by the mp-Patlak method using 30–90 min blood samples, and $V_0 = 0.52$ when using 30–60 min blood samples.

Statistical analysis

Normally distributed results are presented as mean ± standard deviation (SD). Non-normally distributed data are presented as median (25th percentile; 75th percentile).

K_i was independently calculated for mp-Patlak by an experienced nuclear medical specialist (S) and by a medical resident (R) to determine inter-observer variability. The paired t-test was used to compare mean values of K_i and V_0 obtained from the various input functions, where a two-tailed p-value of 0.05 or less was considered statistically significant. Correlations between K_i-values obtained using different analysis models were calculated by linear regression and presented by Pearson's correlation coefficient and the chi^2-test was used to evaluate the fit of the input functions to an applied model. The percentage coefficient of variation of the population residual curves was obtained by dividing the SD by the population residual curve and the 95% confidence interval was estimated using a chi^2 distribution.

Results

The mean plasma to whole blood ratio was 1.17 ± 0.03. The mean recovery-coefficients β were 0.69 ± 0.15 and 1.06 ± 0.44 when the IDAIF was obtained from TACs in the LV and the AO respectively.

Input functions

Figure 5 shows five different AIFs analysed in the present study. The original β-corrected image data resulted in significantly higher values at all time-points, resulting in a larger area under the curve (AUC). Table 2 shows the characteristic mean peak- and AUC-values of the various AIFs before and after β-correction and fitting with the terminal plasma exponentials.

Table 2
Values of all input functions are presented and compared with the β-corrected image-derived arterial input function (IDAIF)

	IDAIF β-corrected	IDAIF Not β-corrected	IDAIF β-corrected and blood samples (30–60 min)	IDAIF β-corrected and blood samples (30–90 min)	SPIF Population residual 2 and blood samples (30–60 min)	SPIF Population residual 2 and blood samples (30–90 min)
Peak value ± SD	169 ± 56	124 ± 41	158 ± 56	145 ± 51	162 ± 36	146 ± 31
- Percentage difference (p-value)	-	-27% (< 0.001*)	-7% (0.124)	-14% (< 0.001*)	-4% (0.665)	-14% (0.137)
AUC ± SD	365 ± 54	311 ± 62	353 ± 59	341 ± 54	348 ± 74	331 ± 70
- Percentage difference (p-value)	-	-15% (< 0.001*)	-3% (0.285)	-7% (< 0.001*)	-5% (0.125)	-9% (0.003*)
mp-Patlak-fit, r^2 ± SD	0.9967 ± 0.002	0.9967 ± 0.002	0.9959 ± 0.002	0.9943 ± 0.003	0.9961 ± 0.002	0.9947 ± 0.002
- Percentage difference (p-value)	-	+ 0% (0.503)	-0.1% (0.106)	0.2% (< 0.001*)	-0.1% (0.157)	-0.2% (< 0.001*)

Data are presented as mean values ± SD obtained by the same 12 scans. The mp-Patlak fit was evaluated by Pearson's correlations coefficient (r^2). *Level of statistical significance is $p < 0.05$

Table 3 evaluates the various input curves by comparing their terminal exponentials with the terminal exponential of the plasma samples and found only small average differences in activity values at all comparable time-points.

Table 3
Comparison of the terminal exponentials of blood samples and image-derived input curves with and without β-correction

	TAC obtained from left ventricle			TAC obtained from aorta		
Image-derived terminal exponential	Non-corrected	β-corrected	β-corrected	Non-corrected	β-corrected	β-corrected
Blood sample derived terminal exponential	30, 40, 50, and 60 min	30, 40, 50, and 60 min	30, 40, 50, 60, and 90 min	30, 40, 50 and 60 min	30, 40, 50, and 60 min	30, 40, 50, 60, and 90 min
Mean difference (kBq/min) ± SD	-0.52 ± 1.02	-0.32 ± 0.79	-0.70 ± 0.39	-0.48 ± 1.22	0.40 ± 0.99	-0.03 ± 0.75
p-value	0.105	0.187	< 0.001*	0.224	0.208	0.904
Mean ratio ± SD	0.91 ± 0.17	1.06 ± 0.14	1.13 ± 0.07	0.94 ± 0.19	0.95 ± 0.14	1.02 ± 0.04
p-value	0.111	0.143	< 0.001*	0.307	0.305	0.604

Mean differences significantly different from 0 and mean ratios significantly different from 1 were determined using the student paired t-test. *Level of statistical significance $p < 0.05$

Population residual curves

The various population residual curves are shown in Fig. 6a. The variation in the curves is illustrated by the SD of the residual curves in Fig. 6b (plotted as the percentage of the total population residual curve).

All curves show the highest SD for the peak-time of the population residual curve, most pronounced in population residual 1 with a SD of 59% (95% CI: 41–104%). The lowest variation of the peak (16.5 s) was found in population residual 2 (30% (21–52%)). An average SD of the entire curve was lowest in population residual 2 (Residual 1: 18.5%; Residual 2: 15.8%; Residual 3: 16.2%).

Comparison of the peak-activity values and AUCs of the SPIFs derived by the 2 observers, after combining the population residual curves with the terminal exponentials of the venous plasma samples for 30–60 minutes and 30–90 minutes, is shown in Table 4. No significant differences were observed between the IDAIFs' mean AUC compared to the SPIFs' mean AUC when adding the terminal exponential taken 30–60 minutes after injection. Statistically significant difference was found by observer-R in peak-values for population residual 1, using the 30–90 minute plasma samples as SPIF when compared with IDAIFs using 30–90 minute plasma samples as SPIF, but this difference was not found by observer-S. However, the resulting AUC's were not significantly different.

Table 4
Comparison of AUC and Peak values for the various SPIFs

Observer-R								
First and second exponential	Image-derived, β-corrected	Population residual 1	Population residual 2	Population residual 3	Image-derived, β-corrected	Population residual 1	Population residual 2	Population residual 3
Terminal exponential	Blood samples (30-60 min)				Blood samples (30-90 min)			
AUC ± SD [min x (kBq/cc)]	353 ± 59	366 ± 78	348 ± 74	342 ± 72	341 ± 54	348 ± 74	331 ± 70	324 ± 69
- Percentage difference (p-value)	-	+3.7% (0.345)	-1.4% (0.671)	-3.1% (0.342)	-	+2.1% (0.523)	-2.9% (0.315)	-5.0% (0.103)
Peak value (kBq/cc)	158 ± 56	128 ± 28	162 ± 36	166 ± 36	145 ±51	115 ± 24	146 ± 31	149 ± 31
- Percentage difference (p-value)	-	-19% (0.063)	+3% (0.777)	+5% (0.605)	-	-21% (0.039*)	+0.7% (0.955)	+3% (0.764)

Observer-S								
First and second exponential	Image-derived, β-corrected	Population residual 1	Population residual 2	Population residual 3	Image-derived, β-corrected	Population residual 1	Population residual 2	Population residual 3
Terminal exponential	Blood samples (30-60 min)				Blood samples (30-90 min)			
AUC ± SD [min x (kBq/cc)]	376 ± 66	400 ± 117	385 ± 111	381 ± 111	357 ± 61	366 ± 80	353 ± 76	349 ± 76
- Percentage difference (p-value)	-	+6.4% (0.332)	+2.4% (0.676)	+1.3% (0.809)	-	+2.5% (0.340)	-1.1% (0.659)	-2.2% (0.362)
Peak value (kBq/cc)	189 ± 76	167 ± 72	212 ± 94	229 ± 101	170 ± 66	140 ± 37	177 ± 47	191 ± 51
- Percentage difference (p-value)	-	-12% (0.460)	+12% (0.498)	+21% (0.260)	-	-18% (0.133)	+4% (0.736)	+12% (0.292)

SPIFs were obtained by combination of the population residual curves with the terminal exponential of venous plasma samples obtained at 30-60 minutes or 30-90 minutes post injection and analyzed by two observers: 4a) medical resident (R) and 4b) nuclear medicine specialist (S). Level of statistical significance: $p < 0.05$

Skeletal plasma clearance

Figure 3 shows a typical bone TAC. Initially the tracer concentration is very low and the resulting part of the curve is generally poorly defined, making it difficult, if not impossible, to determine the exact time of arrival of the flow peak. Uptake in bone rises significantly after a few minutes, but with slowly declining rate.

Hawkins model: Non-linear regression analysis

The rate constants (K_1-k_4) were determined using the Hawkins two-tissue compartmental model for the uncorrected and corrected IDAIFs from both the LV and AO. The data shown in Table 5 are calculated with no constraints on K_1/k_2, with K_1/k_2 fixed to a population value of 0.43 [11] and with the present study's population value of 0.51.

For all input functions, the value of k_4 never exceeds 0.011 min^{-1} indicating that – at least within the 60-minute time frame of the dynamic study – the efflux of ^{18}F-NaF from the vertebrae is mostly negligible, an important prerequisite for proper use of the Patlak-analysis method.

Table 5
Results for the rate constants (K_{1-4}) analysed by the Hawkins' two-tissue compartmental model

LV		K_1 (ml min^{-1} ml^{-1})	k_2 (min^{-1})	k_3 (min^{-1})	k_4 (min^{-1})	Chi^2
IDAIF, not ß-corrected	V_0 adjustable	0.144 ± 0.06	0.440 ± 0.31	0.196 ± 0.07	0.008 ± 0.01	44.1 ± 41.2
	V_0: 0.43	0.131 ± 0.05	0.303 ± 0.11	0.205 ± 0.06	0.011 ± 0.01	44.0 ± 40.7
	V_0: 0.51	0.122 ± 0.05	0.238 ± 0.09	0.169 ± 0.05	0.007 ± 0.01	57.0 ± 60.8
IDAIF, ß-corrected	V_0 adjustable	0.111 ± 0.04	0.366 ± 0.26	0.195 ± 0.07	0.005 ± 0.005	60.1 ± 53.4
	V_0: 0.43	0.102 ± 0.04	0.237 ± 0.10	0.192 ± 0.08	0.008 ± 0.01	59.6 ± 52.5
	V_0: 0.51	0.089 ± 0.03	0.174 ± 0.06	0.145 ± 0.06	0.010 ± 0.10	57.5 ± 61.2

AO		K_1 (ml min^{-1} ml^{-1})	k_2 (min^{-1})	k_3 (min^{-1})	k_4 (min^{-1})	Chi^2
IDAIF, not ß-corrected	V_0 adjustable	0.113 ± 0.04	0.377 ± 0.23	0.189 ± 0.07	0.009 ± 0.01	47.8 ± 39.6
	V_0: 0.43	0.102 ± 0.03	0.243 ± 0.07	0.194 ± 0.06	0.011 ± 0.01	47.6 ± 39.1
	V_0: 0.51	0.093 ± 0.03	0.494 ± 0.07	0.145 ± 0.05	0.001 ± 0.003	56.3 ± 55.9
IDAIF, ß-corrected	V_0 adjustable	0.122 ± 0.07	0.373 ± 0.40	0.191 ± 0.15	0.002 ± 0.004	56.6 ± 55.2
	V_0: 0.43	0.115 ± 0.07	0.267 ± 0.17	0.180 ± 0.07	0.003 ± 0.01	55.6 ± 54.4
	V_0: 0.51	0.109 ± 0.07	0.214 ± 0.13	0.152 ± 0.06	0.002 ± 0.01	55.9 ± 54.3

Goodness-of-fit for the curves was evaluated by chi^2-test. Values from 12 scans are expressed as mean ± SD. Image-derived AIFs (IDAIFs) were obtained from: 5a) TAC of left ventricle of the heart (LV) 5b) TAC of thoracic aorta (AO). V_0 (K_1/k_2) was adjustable, fixed to a previously published population value of 0.43 or our own value of 0.51 obtained by Hawkins analysis.

Patlak: multiple-point graphical analysis

All dynamic datasets analysed according to Eq. 3 showed excellent straight line fits with linear correlation coefficients close to 1.0 (LV: R^2 = 0.997 ± 0.001; AO: R^2 = 0.995 ± 0.003).

Table 6 presents comparison of K_i and V_0 values obtained from non-linear regression analysis and mp-Patlak analysis when using IDAIFs derived from LV, AO and SPIF. The difference between the K_i-values using various dynamic input functions, with or without blood sampling within the same time period, was not statistically significant.

Table 6

Comparison of K_i-values and V_0-values obtained by the Hawkins method and Patlak multi-point analysis using various IDAIFs

LV	Hawkins two-tissue compartmental model				Patlak multi point analysis				
	Raw IDIF	ß-corrected IDIF	ß-corrected IDIF	ß-corrected IDIF	ß-corrected IDAIF	ß-corrected IDAIF and blood samples 30-60 min	ß-corrected IDAIF and blood samples 30-90 min	SPIF, population residual 2 and blood samples 30-60 min	SPIF, population residual 2 and blood samples 30-90 min
	V_0 adjustable	V_0 adjustable	V_0 0.43	V_0 0.51	V_0 adjustable	V_0 adjustable	V_0 adjustable	V_0 adjustable	V_0 adjustable
K_i, (ml min^{-1} ml^{-1}) ±SD	0.0480 ± 0.014	0.0415 ± 0.013	0.0424 ± 0.013	0.0379 ± 0.010	0.0337 ± 0.009	0.0341 ± 0.009	0.0342 ± 0.009	0.0340 ± 0.008	0.0346 ± 0.009
- Percentage difference (P-value)					-	+1.2% (0.604)	+1.5% (0.043*)	+0.9% (0.718)	+2.7% (0.315)
V_0 ±SD	0.57 ± 0.30	0.51 ± 0.22	-	-	0.39 ± 0.17	0.47 ± 0.26	0.57 ± 0.26	0.52 (± 0.25)	0.64 (± 0.27)

AO	Hawkins two-tissue compartmental model				Patlak multi point analysis				
	Raw IDIF	ß-corrected IDIF	ß-corrected IDIF	ß-corrected IDIF	ß-corrected IDAIF	ß-corrected IDAIF and blood samples 30-60 min	ß-corrected IDAIF and blood samples 30-90 min	SPIF, population residual 2 and blood samples 30-60 min	SPIF, population residual 2 and blood samples 30-90 min
	V_0 adjustable	V_0 adjustable	V_0 0.43	V_0 0.51	V_0 adjustable	V_0 adjustable	V_0 adjustable	V_0 adjustable	V_0 adjustable
K_i, ml min^{-1} ml^{-1} ±SD	0.0414 ± 0.007	0.0382 ± 0.009	0.0399 ± 0.010	0.0389 ± 0.010	0.0338 ± 0.009	0.0325 ± 0.010	0.0333 ± 0.010	0.0322 ± 0.008	0.0331 ± 0.009
V_0 ±SD	0.57 ± 0.24	0.46 ± 0.24	-	-	0.43 ± 0.24	0.41 ± 0.26	0.49 ± 0.27	0.39 ± 0.22	0.50 ± 0.25

Mean ± SD from 12 scans (Th7-10). The Hawkins analysis was made with an adjustable V_0-value, with a fixed population value of 0.43 and our own population value of 0.51. *Level of statistical significance is $p < 0.05$. Image-derived AIFs (IDAIFs) were obtained from: 6a) TAC of left ventricle of the heart (LV) and 6b) TAC of thoracic aorta (AO).

Comparison of K_i results between non-linear regression analysis and mp-Patlak analysis using β-corrected IDAIF in combination with 30–90 min blood samples (Fig. 7a), shows a statistically significant linear correlation ($R^2 = 0.92$, $p < 0.001$). Similarly, a statistically significant correlation was found between Hawkins and mp-Patlak K_i-values using β-corrected IDAIF plus 30–60 min blood samples ($R^2 = 0.93$, $p < 0.001$).

No significant inter-observer differences in the K_i-values obtained with use of mp-Patlak analysis were found (Table 7).

Table 7

Comparison of K_i-values (ml min^{-1} ml^{-1}) analyzed by a nuclear medical specialist (S) and a medical resident (R)

	S	R	p-value
IDAIF	0.0317 ± 0.009	0.0337 ± 0.009	0.108
IDAIF + blood samples (30–60 min)	0.0320 ± 0.009	0.0341 ± 0.009	0.092
IDAIF + blood samples (30–90 min)	0.0323 ± 0.010	0.0342 ± 0.009	0.153

All K_i-values are a mean value from 12 scans (Th7-10) by Patlak multi point analysis. β-corrected image-derived AIFs (IDAIF) are obtained from TACs of left ventricle with and without addition of the terminal exponential from blood samples (30–60 minutes or 30–90 minutes).

Patlak: single-point graphical analysis

Table 8 shows K_i-values obtained by sp-Patlak analysis. For this analysis a SPIF constructed of population residual 2 in combination with the terminal exponential of plasma samples taken at 30–60 minutes or 30–90 minutes was used.

Table 8
K_i-results obtained using the static whole-body single-point Patlak analysis (sp-Patlak)

Analyses model	First and second exponential	Terminal exponential	V_0, (%)	K_i (ml min^{-1} ml^{-1})	Percentage difference	p-value	R	p-value
mp-Patlak	Population residual 2	Blood samples 30–90 min	**64**	**0.0346 ± 0.009**	-	-	-	-
sp-Patlak	Population residual 2	Blood samples 30–60 min	43	0.0399 ± 0.010	+ 15%	< 0.001*	0.930	< 0.001*
			52	0.0390 ± 0.010	+ 13%	0.002*	0.931	< 0.001*
sp-Patlak	Population residual 2	Blood samples 30–90 min	43	0.0419 ± 0.011	+ 21%	< 0.001*	0.940	< 0.001*
			64	0.0395 ± 0.011	+ 14%	0.001*	0.942	< 0.001*

Mean values ± SD are presented from 12 scans (Th7-10). Three different assumptions of V_0 are applied and compared with multi-point Patlak (mp-Patlak) values obtained using dynamic analysis. Pearson's correlation coefficient (R), *Level of Statistically significance: $p < 0.05$

Figure 7b shows statistically significant correlation between mp-Patlak and sp-Patlak mean K_i-values using SPIF with population residual 2 and 30–90 minute blood samples ($R = 0.94$, $p < 0.001$), which was not observed when using 30–60 minute blood samples.

Discussion

Methods for assessing skeletal health which can replace the gold standard bone biopsy are sorely needed in the clinical CKD-MBD setting, e.g. effective and necessary bone treatment may be withheld if a patient has suspect adynamic bone. Access to non-invasive diagnostic methods to confirm or negate this would be an important clinical gain. This study implements both dynamic and static ^{18}F-NaF PET/CT imaging using multiple kinetic analysis methods: non-linear regression, Patlak multi- and single-point analysis, as well as determines a representative CKD-MBD SPIF for use with static PET data, for comparison of the various techniques. All presented methods are suitable for skeletal plasma clearance evaluation, where the simplified Patlak and WB PET methods are suitable for implementation in clinical practice, with static WB ^{18}F-NaF PET/CT opening up possibilities for easy clinical assessment of skeletal health in CKD-MBD.

To some extent CKD-MBD is present in all patients suffering from severe kidney failure in need of dialysis treatment. Therefore, the present study includes chronic dialysis patients as representatives of the CKD-MBD population. The participants in the present study were mostly males (70%) and diabetic nephropathy was the most common cause of kidney failure (29%). Previous studies using ^{18}F-NaF PET/CT for dynamic bone examination have mostly studied female osteoporotic patients and excluded patients with CKD [16, 12]. However, a recently published study of a CKD-MBD population also included 50% males with diabetic nephropathy as the most common cause of kidney failure (34%) [17].

Input functions

Ideally, an AIF should be derived from the arteria supplying the bone region of interest by direct arterial sampling. However, an image-derived AIF is known to be a good approximation of an AIF [10]. In the past years, research in osteoporosis has frequently used ^{18}F-NaF PET/CT quantitative analysis, where the most common region to obtain the IDAIF has been a TAC derived from the abdominal aorta feeding the nearby bone regions. However, use of the abdominal aorta for the AIF has some limitations: the AUC is underestimated when using the abdominal aorta TAC compared with direct arterial sampling [14] and the abdominal aorta is not always close to the bone-of-interest in a whole-body scan. In addition, the aorta is often calcified and twisted in the elderly CKD-MBD population [18], which results in VOIs placed in the aorta being more sensitive to local variable flow patterns and thus local variations in radioactive concentration. In comparison, a VOI placed in the LV allows the definition of large VOIs which will be much less sensitive to partial-volume-effects as well as local flow and radioactive concentration variations. Thus, the LV may provide the most universal activity pool for use with extended WB anatomical regions-of-interest studies. In the present study IDAIFs are obtained from LV TACs, but the results from AO TACs have also been measured for comparison with previous results. It was observed that LV VOIs performed better than VOIs placed in the AO.

The present study evaluates several different input functions (Fig. 5). All IDAIFs were converted to plasma activity using the average plasma to whole blood ratio found by venous blood sampling as described by Cook et al. [10]. In this present study, we find the plasma/whole blood ratio to be slightly

lower, where some of the difference may be explained by renal anemia in the CKD-MBD population. As we did not have arterial plasma samples, we were unable to correct for changes in the plasma/whole blood ratio over time as done by Cook et al. [10].

The recovery coefficient β was calculated to correct the IDAIF for PVE and spillover between activity in the lumen and background structures (β-corrected IDAIF). We found the variation of this β-coefficient to be slightly dependent on image quality but even more sensitive to blood sampling errors. Hence, optimal blood sampling is particularly important to obtain a reliable β-correction. The mean AUC of a β-corrected IDAIF has previously been shown to be comparable with the AUC from direct arterial sampling[14] and as such, the β-corrected IDAIF was chosen as our reference input function for comparison with results from other input functions.

The mean β-coefficient was lower (0.69 ± 0.15) when the IDAIFs were derived from the LV as compared with the AO (1.06 ± 0.44). These findings suggest that β-correction is required with LV derived input functions, but not for AO input functions. The higher AO β-coefficient results from a low background activity and is found to be in the same range as previously published values for correction of AO (0.97 ± 0.54) [14].

The effect of applying the various corrections to the input curves has been compared. The mean AUC and mean peak-value were significantly lower for uncorrected IDAIF compared with β-corrected IDAIF (Table 2). Consequently, using an IDAIF without β-correction will result in higher K_i-results (0.0480 ml min^{-1} ml^{-1}) compared to results from a β-corrected IDAIF (K_i = 0.0415 ml min^{-1} ml^{-1}) as shown in Table 6. However, the results were not significantly different (p = 0.06).

β-corrected IDAIF combined with blood sample adjustment results in a slightly lower mean AUC than β-corrected IDAIFs alone. This difference is statistically significant when the 30–90 minute blood samples are used. Nevertheless, the difference seems to be in an acceptable range (Table 2). Likewise, K_i-results are higher when β-corrected IDAIFs adjusted by venous blood samples are used, compared to β-corrected IDAIF, as the input function. Again, a statistically significant difference is observed for the 30–90 minute blood samples with an acceptably low (1.5%) difference. The reason for this is possibly due to steady-state NaF distribution not being reached by 60 minutes, and thus we can expect slight differences between plasma curves fitted to data at 60 minutes and 90 minutes.

To enable future sp-Patlak analysis of multiple bone regions from a single static WB scan, a SPIF combining population residual 2 (having lowest SD) and venous blood samples for an AIF was derived. Once more, the AUC is found to be slightly, but insignificantly, lower than that of the β-corrected IDAIF AUC, resulting in higher K_i-results (Table 6).

Table 4 compares differences in mean AUC and mean peak-values when the first and second exponentials are obtained from image-derived or population residual curves. AUCs show no statistically significant differences. This suggests it is feasible for a fully dynamic IDAIF to be replaced by a generalized SPIF for estimation of dynamic information in bone clearance studies, which is necessary for investigation of extended, multiple bone regions.

V_0 is observed to vary with the choice of input function and analysis model as shown in Table 6. Using the Hawkins compartmental model with β-corrected IDAIF gives a mean V_0 value of 0.51. Correspondingly a value of 0.39 is found for mp-Patlak analysis with the same input function, or 0.43 when the AO TAC, instead of the LV TAC, is applied for the β-corrected IDAIF. This AO value is comparable to the population value previously reported by Siddique et al [11] in a population of 10 women with osteoporosis. Additionally, when SPIFs are used for the mp-Patlak analysis, mean V_0-values tend to be comparable or even higher. For sp-Patlak, Siddique et al have previously published a V_0 of 0.46 when using a SPIF [19].

The value of V_0 is known to be skeletal site, treatment and analysis model specific [11, 19, 20]. However, K_i estimates have been shown to be relatively independent of the choice of V_0. A 20% difference in V_0 resulted in only a 5% change in K_i [11], making the sp-Patlak analysis robust for clinical use, despite variability in the population V_0-value.

Population residual curves

This study investigated three different population residual curves resulting in population residual 2, with the smallest variation, chosen for use in sp-Patlak analysis.

The standard deviation is generally high in all population residual curve models (Fig. 6). However, the coefficients of variation are only slightly higher at the peak than previously published data and lower at the third exponential [9]. In this study, the ^{18}F-NaF tracer was administered by manual bolus injection. It may be possible to produce a population residual curve with even more reduced variation through use of an automated injection system.

Skeletal plasma clearance

Greatest variability in the bone TACs occurs at initial uptake when the measured activity is low (Fig. 3), making it very difficult to accurately determine the exact time of arrival of tracer to the bone. As a consequence, attempts to correct for time delay failed to improve our data. Other published studies have used an average TAC over all vertebra to be investigated and longer time-bins for each frame, which will improve counting statistics but will lower the time resolution and as such may be counterproductive[11, 12]. However, this problem did not affect the Patlak analysis, as the data was sampled at a later time between 14–60 minutes.

Hawkins model: Non-linear regression analysis

The mean K_i-value was 0.042 ± 0.01 ml min^{-1} ml^{-1} applying β-corrected IDAIFs in the Hawkins two-tissue compartment model (Table 6).

The first quantitative ^{18}F-NaF study evaluating kinetics in renal osteodystrophy, reported a mean K_i-value of 0.071 ± 0.03 ml min^{-1} ml^{-1} [5]. A reason for such a high value may, in part, be that 72% of the population studied had untreated secondary hyperparathyroidism. Correspondingly, a new study by Aaltonen et al reported a mean value of 0.067 in dialysis patients with high turnover bone disease and 0.038 in dialysis patients with low turnover bone disease [17]. In comparison, our value of 0.042 ml min^{-1} ml^{-1} lies within the lower cut-off limit defined in the Aaltonen study and above the value reported for two patients with hyperparathyroidism as found by Schiepers et al. (0.034 ml min^{-1} ml^{-1}). Additionally, the latest study looking at K_i related to Paget disease, has published a much higher mean value of 0.114 ml min^{-1} ml^{-1} [21].

Patlak: multiple-point graphical analysis

This study finds a statistically significant correlation between the K_i-values obtained using non-linear regression analysis and mp-Patlak analysis (R: 0.92, p-value: 0.001) (Fig. 7a), similar to previously published K_i-values in a healthy female population and in a postmenopausal female population with osteoporosis [16, 22].

The mean K_i-value is 0.034 ± 0.01 ml min^{-1} ml^{-1} using β-corrected IDAIFs as input to the mp-Patlak analysis. This is similar to results published for a chronic dialysis population (L_{1-4}) with a mean value of 0.039 ml min^{-1} ml^{-1} and, as expected, higher than the mean value of 0.028 ml min^{-1} ml^{-1} found for a hemodialysis population with suspected adynamic bone disease (L_{1-4}) [17, 23].

The mean K_i-value is significantly lower when analyzed using the mp-Patlak method than with the Hawkins two-tissue compartmental model (Table 6). The mean average difference between K_i-values for the two methods is 19% using β-corrected IDAIFs. This difference was reported to be 28.6% by Installé J. et al and 13% by Puri et al. [16, 24].

Previously, it has been suggested that mp-Patlak results are lower than those derived from the Hawkins two-tissue compartmental model due to efflux of tracer from the bone during the scan. If such efflux is present, it may be corrected by the method described by Siddique et al [19]. Since additional investigation showed the Patlak data including later time-point data from the WB scans fit very well to a straight line with regression coefficients close to 1, and taken together with k_4-values ≤ 0.011, we found it unnecessary to correct for efflux in this study.

The mp-Patlak analysis has been reported to be superior to the Hawkins two-tissue compartmental model for research purposes; mp-Patlak analysis is computationally simpler and a lower number of participants are required to show a statistically significant result due to small precision error combined with a large treatment response [15, 22]

In addition, as the K_i-values using the various input functions (Table 6) are not significantly different, our data strongly suggests that dynamic analysis using image derived input functions without blood sampling is feasible for clinical analysis, under the prerequisite that the scanner is accurately cross-calibrated.

Accordingly, we find the mp-Patlak results in the present study to be very robust with no inter-observer significant difference (Table 7).

Patlak: single-point graphical analysis

Using the sp-Patlak analysis with a SPIF as described above for the four vertebrae Th7-Th10 imaged in static WB scans, we found the K_i-value to be 0.0395 ± 0.011 ml min^{-1} ml^{-1}. Unsurprisingly, the K_i-result in the present study is higher than the K_i-result from a previous published study in patients with suspected adynamic bone disease (0.028 ± 0.012 ml min^{-1} ml^{-1}). For comparison, the K_i-result in a study of patients with osteoporosis was in the lower range with a value of 0.025 ± 0.007 ml min^{-1} ml^{-1} [22, 23].

Comparing K_i-results from the sp-Patlak analysis with K_i-results from the mp-Patlak analyses using the same input functions, resulted in 14% higher K_i-results ($p < 0.001$). Despite this, the correlation between the methods is very good ($R^2 = 0.942$, $P < 0.001$). This however, emphasizes the importance of using the same analysis method when comparing results of tracer kinetic parameters.

Conclusion

Three different methods for analysis of skeletal plasma clearance in a population of CKD-MBD patients for both experimental and clinical use using ^{18}F-NaF PET/CT scan have successfully been implemented.

A dynamic scan protocol using the Hawkins two-tissue compartmental model with reliable mean K_i- and K_{1-4}-values has been established. As expected, the K_i-values are lower using mp-Patlak analysis compared with Hawkins two-tissue compartmental model analysis.

A CKD-MBD population residual curve and SPIF have been developed for use with WB PET/CT scans, allowing site-specific measurements of bone formation in multiple regions. Variation in a constructed population curve can be minimized using LV as IDAIF and with adjustment of individual peak

times to the most frequent unadjusted peak time.

Skeletal plasma clearance values reported in the present study are comparable with previously published values for various patient populations but vary with the analysis method used. Comparison with bone biopsy is required to further validate bone turnover measurements determined from ^{18}F-NaF PET/CT scans in CKD-MBD patients.

Declarations

Ethical approval and consent to participate

All procedures performed in studies involving human participants were in accordance with the ethical standards of the institutional and/or national research committee and with the 1964 Helsinki declaration and its later amendments or comparable ethical standards. The study was approved by the Regional Committee on Biomedical Research Ethics (case number: 1-10-72-340-16) and Danish Health and Medicines Authority, EudraCT number: 2016-005160-34.

Informed consent was obtained from all individual participants included in the study.

Consent to publication

Informed consent was obtained from all participants regarding publishing of data

Availability of data and material

The datasets used and analysed during the current study are available from the corresponding author on reasonable request.

Competing interests

The authors declare that they have no conflict of interest.

Funding

This study was funded by the Danish Kidney Association's Research Fund, The Axel Muusfeldt Foundation and Health Research Foundation of the Central Denmark Region.

Authors' contributions

Study design: MV, JT, CF, TGL, JB

Study execution: MV, TGL, CF, JB

Method implementation, creation & validation of analysis tools: CF, JT

Image analysis: MV, JT, CF

Statistical analysis: MV

First draft: MV

Manuscript review and approved: all authors

Acknowledgements

The authors thank Malene Skov Hansen and Mette Emtkjær Mølgaard for their invaluable help with the practical execution of the PET/CT scans and blood sample analyses.

References

1. Blau M, Nagler W, Bender MA. Fluorine-18: a new isotope for bone scanning. Journal of nuclear medicine: official publication Society of Nuclear Medicine. 1962;3:332–4.

2. Moe S, Drueke T, Cunningham J, Goodman W, Martin K, Olgaard K, et al. Definition, evaluation, and classification of renal osteodystrophy: a position statement from Kidney Disease: Improving Global Outcomes (KDIGO). Kidney international. 2006;69(11):1945–53. doi:S0085-2538(15)51415-4 [pii].
3. Lucas RC. On a form of late rickets associated with albuminuria, rickets of adolecents. Lancet. 1883;1:993–4.
4. KDIGO. 2017 Clinical Practice Guideline Update for the Diagnosis, Evaluation, Prevention, and Treatment of Chronic Kidney Disease-Mineral and Bone Disorder (CKD-MBD). Kidney international supplements. 2017;7(1):1–59.
5. Messa C, Goodman WG, Hoh CK, Choi Y, Nissenson AR, Salusky IB, et al. Bone metabolic activity measured with positron emission tomography and [18F]fluoride ion in renal osteodystrophy: correlation with bone histomorphometry. J Clin Endocrinol Metab. 1993;77(4):949–55. doi:10.1210/jcem.77.4.8408470 [doi].
6. Blau M, Ganatra R, Bender MA. 18 F-fluoride for bone imaging. New York:: W B Saunders; 1972. pp. 31–7.
7. Hawkins RA, Choi Y, Huang SC, Hoh CK, Dahlbom M, Schiepers C, et al. Evaluation of the skeletal kinetics of fluorine-18-fluoride ion with PET. Journal of nuclear medicine: official publication. Society of Nuclear Medicine. 1992;33(5):633–42.
8. Patlak CS, Blasberg RG, Fenstermacher JD. Graphical evaluation of blood-to-brain transfer constants from multiple-time uptake data. Journal of cerebral blood flow metabolism: official journal of the International Society of Cerebral Blood Flow Metabolism. 1983;3(1):1–7. doi:10.1038/jcbfm.1983.1 [doi].
9. Blake GM, Siddique M, Puri T, Frost ML, Moore AE, Cook GJ, et al. A semipopulation input function for quantifying static and dynamic 18F-fluoride PET scans. Nucl Med Commun. 2012;33(8):881–8. doi:10.1097/MNM.0b013e3283550275 [doi].
10. Cook GJ, Lodge MA, Marsden PK, Dynes A, Fogelman I. Non-invasive assessment of skeletal kinetics using fluorine-18 fluoride positron emission tomography: evaluation of image and population-derived arterial input functions. Eur J Nucl Med. 1999;26(11):1424–9. doi:90261424.259 [pii].
11. Siddique M, Blake GM, Frost ML, Moore AE, Puri T, Marsden PK, et al. Estimation of regional bone metabolism from whole-body 18F-fluoride PET static images. Eur J Nucl Med Mol Imaging. 2012;39(2):337–43. doi:10.1007/s00259-011-1966-y [doi].
12. Frost ML, Siddique M, Blake GM, Moore AE, Schleyer PJ, Dunn JT, et al. Differential effects of teriparatide on regional bone formation using (18)F-fluoride positron emission tomography. Journal of bone mineral research: the official journal of the American Society for Bone Mineral Research. 2011;26(5):1002–11. doi:10.1002/jbmr.305 [doi].
13. Mizobuchi M, Towler D, Slatopolsky E. Vascular calcification: the killer of patients with chronic kidney disease. J Am Soc Nephrol. 2009;20(7):1453–64. doi:10.1681/ASN.2008070692.
14. Puri T, Blake GM, Siddique M, Frost ML, Cook GJR, Marsden PK, et al. Validation of new image-derived arterial input functions at the aorta using 18F-fluoride positron emission tomography. S.l.]:: Lippincott; 2011. pp. 486–95.
15. Brenner W, Vernon C, Muzi M, Mankoff DA, Link JM, Conrad EU, et al. Comparison of different quantitative approaches to 18F-fluoride PET scans. Journal of nuclear medicine: official publication. Society of Nuclear Medicine. 2004;45(9):1493–500. doi:45/9/1493 [pii].
16. Puri T, Blake GM, Frost ML, Siddique M, Moore AE, Marsden PK, et al. Comparison of six quantitative methods for the measurement of bone turnover at the hip and lumbar spine using 18F-fluoride PET-CT. Nucl Med Commun. 2012;33(6):597–606. doi:10.1097/MNM.0b013e3283512adb.
17. Aaltonen L, Koivuviita N, Seppanen M, Tong X, Kroger H, Loyttyniemi E, et al. Correlation between (18)F-Sodium Fluoride positron emission tomography and bone histomorphometry in dialysis patients. Bone. 2020;134:115267. doi:10.1016/j.bone.2020.115267.
18. Garcia J, van der Palen RLF, Bollache E, Jarvis K, Rose MJ, Barker AJ, et al. Distribution of blood flow velocity in the normal aorta: Effect of age and gender. J Magn Reson Imaging. 2018;47(2):487–98. doi:10.1002/jmri.25773.
19. Siddique M, Frost ML, Moore AE, Fogelman I, Blake GM. Correcting (18)F-fluoride PET static scan measurements of skeletal plasma clearance for tracer efflux from bone. Nucl Med Commun. 2014;35(3):303–10. doi:10.1097/MNM.0000000000000047 [doi].
20. Blake GM, Siddique M, Frost ML, Moore AE, Fogelman I. Imaging of site specific bone turnover in osteoporosis using positron emission tomography. Curr Osteoporos Rep. 2014;12(4):475–85. doi:10.1007/s11914-014-0231-2.
21. Christiaan Schiepers JN, Guy Bormans J, Dequeker R, Bouillon L, Mortelmans. Alfons Verbruggen and Michel De Roo. Fluoride Kinetics of the Axial Skeleton Measured in Vivo with Fluorine-18-Fluoride PET. The Journal of Nuclear Medicin. 1997;38(12):1970–6.
22. Siddique M, Frost ML, Blake GM, Moore AEB, Al-Beyatti Y, Marsden PK, et al. The precision and sensitivity of (18)F-fluoride PET for measuring regional bone metabolism: a comparison of quantification methods. 2011. p. 1748–55.
23. Frost ML, Compston JE, Goldsmith D, Moore AE, Blake GM, Siddique M, et al. (18)F-fluoride positron emission tomography measurements of regional bone formation in hemodialysis patients with suspected adynamic bone disease. Calcif Tissue Int. 2013;93(5):436–47. doi:10.1007/s00223-013-9778-7 [doi].
24. Installé J, Nzeusseu A, Bol A, Depresseux G, Devogelaer J-P, Lonneux. M. ^{18}F-Fluoride PET for Monitoring Therapeutic Response in Paget's Disease of Bone. J Nucl Med. 2005;46(10).

Figures

Figure 1

Title: Two-tissue, three compartmental model Legend: The two-tissue, three compartmental model as described by Hawkins et al. [7]

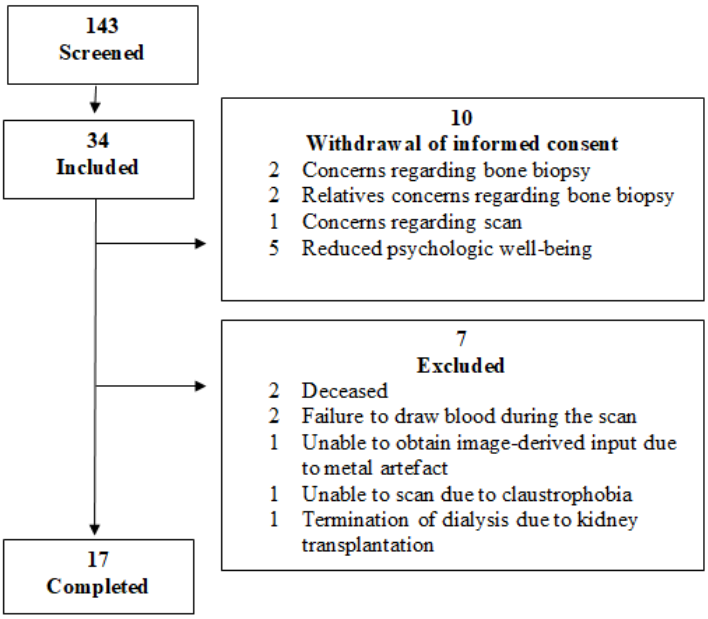

Figure 2

Title: Flowchart of participant recruitment. Legend: Patients were additionally screened to participate in a bone biopsy as part of the complete study. Concerns regarding the bone biopsy contributed largely to the large withdrawal of consent seen in this study.

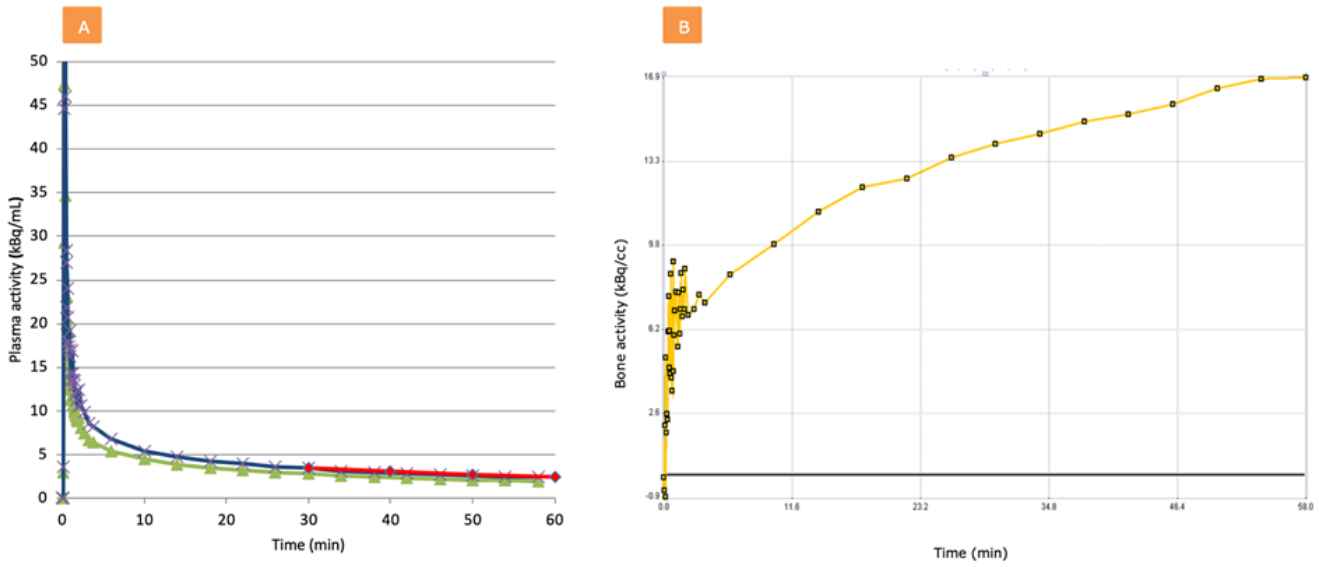

Figure 3

Title: Example data curves obtained in the present study (participant no.32). Legend: 3a) Green line: plasma corrected image-derived AIF (IDAIF). Red line: The terminal exponential obtained from venous blood samples at 30, 40, 50 and 60 minutes. Blue line: β-corrected IDAIF. 3b) Bone TAC obtained from a VOI in vertebra Th7. Noise in the initial part of the curve is caused by low activity in the early time-frames of the study

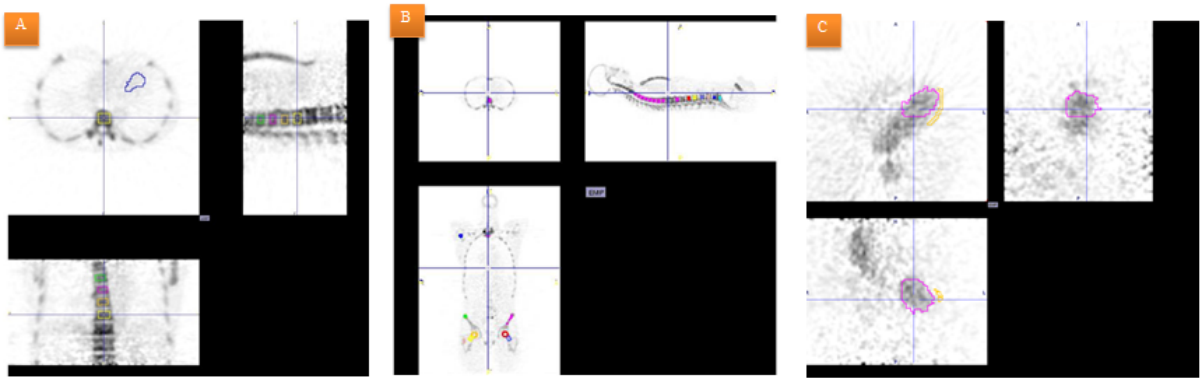

Figure 4

Title: PET-images from dynamic and WB 18F NaF PET/CT scans Legend: a) FOV from a dynamic 18F NaF PET/CT showing VOIs to obtain bone TACs in vertebrae th7-10 and a VOI in the left ventricle of the heart (LV) to obtain the image-derived input function. b) The whole-body 18F NaF PET/CT with the possibility to make bone VOIs in the entire skeleton. c) A VOI placed in LV and a myocardial VOI for β-correction

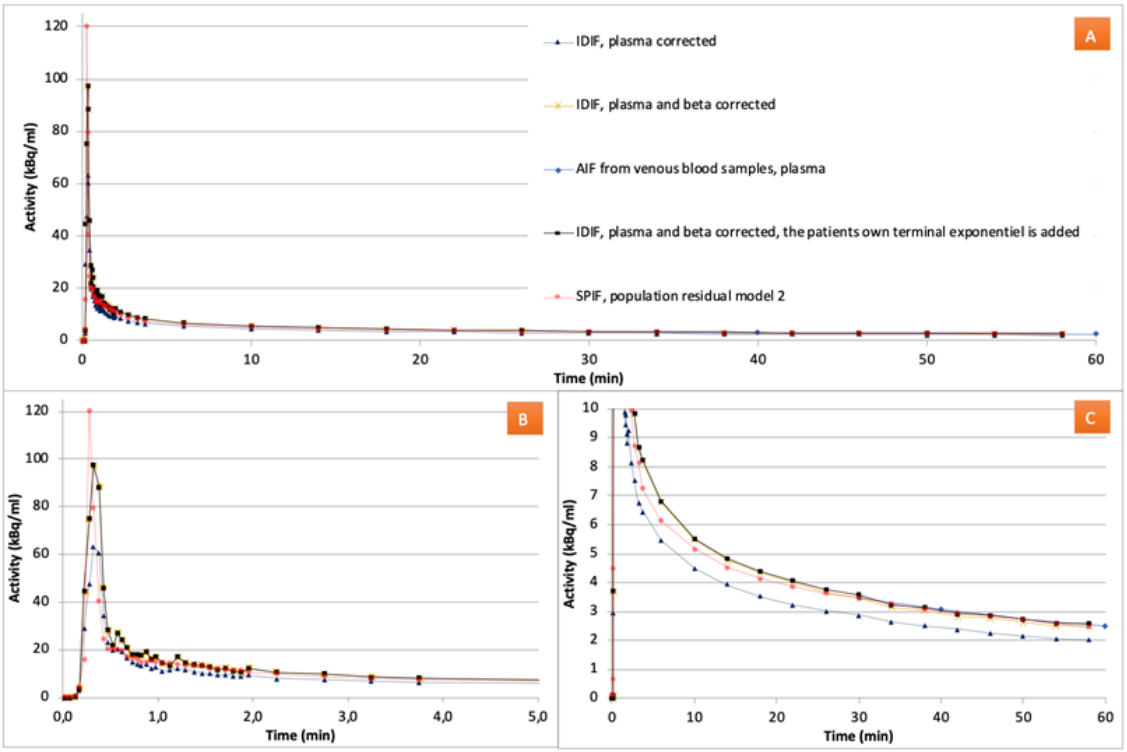

Figure 5

Title: Various input functions Legend: a) Various estimates of the AIFs obtained from example participant (no. 32). b) X-axis is scaled for better visualization of the two first exponentials. c) Y-axis is scaled for better visualization of the terminal exponentials

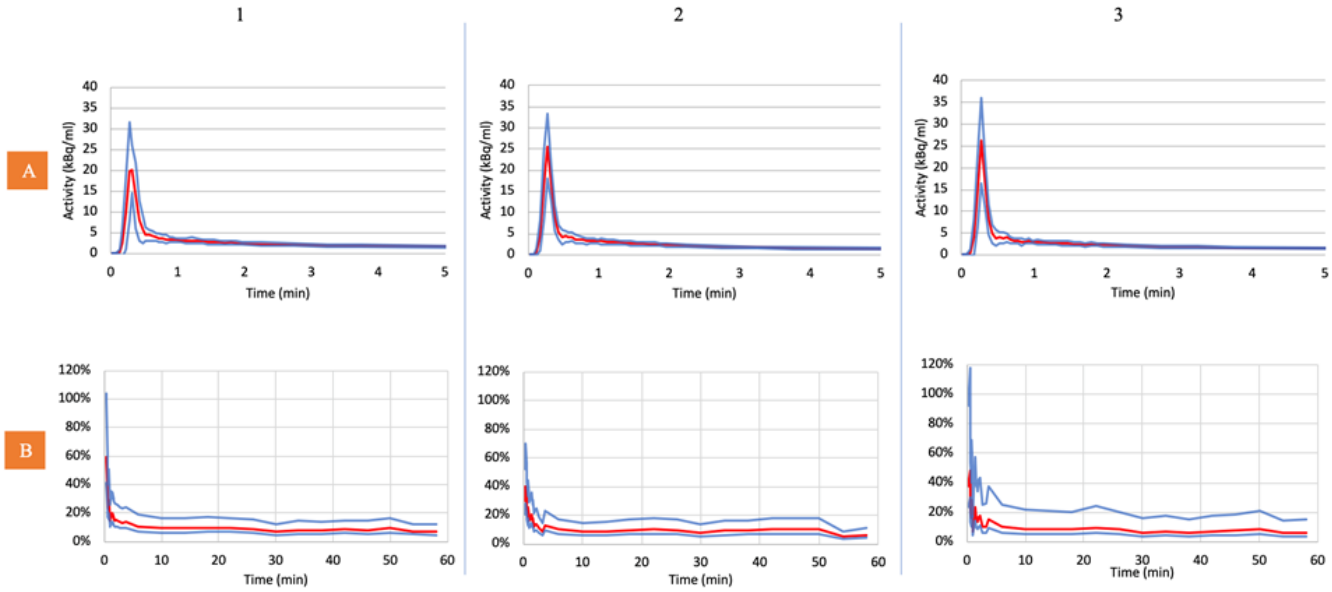

Figure 6

Title: Population residual curves Legend: a) Population residuals 1-3 (red lines) ± 1SD (blue lines). All curves are normalized to a reference activity of 150 MBq. b) The corresponding population SDs (red lines) plotted as the percentage coefficient of variation obtained by dividing the SD by the population residual curve with 95% confidence intervals (blue lines) estimated using the chi² distribution

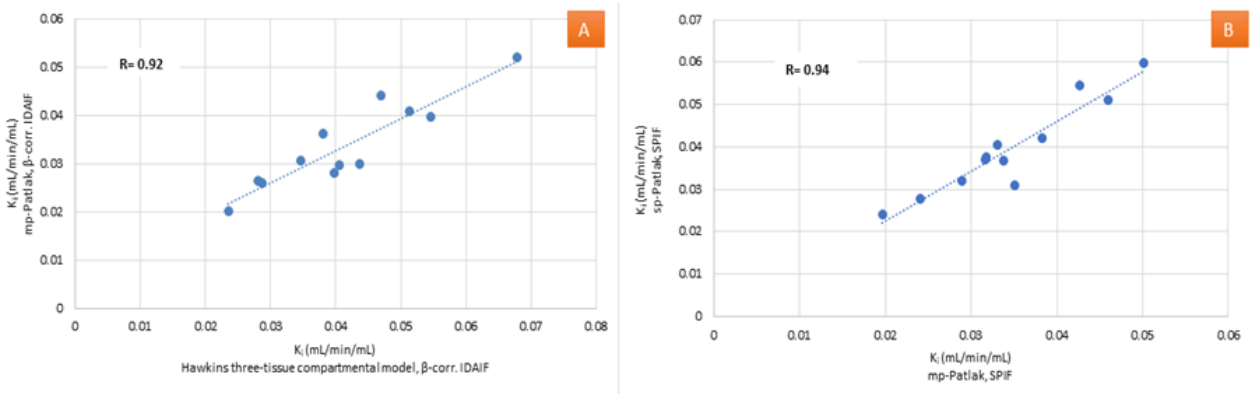

Figure 7

Title: Correlation between Ki values obtained by different analysis models Legend: a) Correlation between mean Ki values obtained by Hawkins two-tissue compartmental model and Patlak multi point analysis (mp-Patlak). b) Correlation between mean Ki value obtained by dynamic mp-Patlak and static whole-body result obtained by single point Patlak analysis method (sp-Patlak)